Integrated genetic and computation methods for *in planta* cytometry

Fernán Federici[1,6], Lionel Dupuy[2,6], Laurent Laplaze[3], Marcus Heisler[4,5] & Jim Haseloff[1]

We present the coupled use of specifically localized fluorescent gene markers and image processing for automated quantitative analysis of cell growth and genetic activity across living plant tissues. We used fluorescent protein markers to identify cells, create seeds and boundaries for the automatic segmentation of cell geometries and ratiometrically measure gene expression cell by cell in *Arabidopsis thaliana*.

A major challenge in developmental biology is to understand genetic and biophysical mechanisms that guide cell growth and self-organization during organogenesis. Studies of such complex mechanisms rely on computer-aided analysis and mathematical modeling of microscopy data. The quantitative analysis of image data generally requires manual extraction of parameters for cell growth and gene activity in intact living tissues. Automated measurement of gene activity and cellular geometry would contribute to better models of morphogenesis. The generation of multiple spectral variants of fluorescent proteins and the development of more powerful image-analysis algorithms and hardware has considerably expanded the scope of automation and information processing in microscopy[1–4]. We exploited these technical advances for simultaneous quantitative analysis of cell topology, size, shape and gene activity from *in vivo* images of plant tissues, using an automated and open-source computational procedure.

Our procedure, which we term *in planta* cytometry, allowed the measurement of cellular properties in intact tissue while retaining the cellular context for subsequent studies. The routine consists of three automated steps. First, we used a genetic marker to specifically label nuclei, index cells and extract positional information using a particle search algorithm (**Fig. 1a**). Second, we used identified nuclei to initiate an active contour segmentation algorithm[5] that used a fluorescent signal located at the plasma membrane to extract information regarding cell size, shape and topology (**Fig. 1b**). Third, we quantified cell-specific gene expression by ratiometric measurement of spectrally distinct nuclear fluorescent proteins expressed under the control of different regulated promoters.

We produced transgenic *Arabidopsis* plants that expressed spectrally distinct fluorescent proteins in cell nuclei and plasma membranes (**Fig. 1c–e**), imaged plant tissues with confocal laser scanning microscopy and subjected them to the procedure outlined above. We used the identified nuclei as seeds for a two-phase active contour segmentation, to define cell shapes in the tissue (**Fig. 1f**). First, our method makes use of inflated balloon-like structures, each of which comprises connected vertices that define an envelope. During the segmentation process, the balloons are gradually inflated and subsequently constrained by the application of external forces from pixel intensities at cell boundaries (fluorescent proteins localized to the plasma membrane). The expansion process is stopped when balloons come in contact with each other or when the balloon internal pressure, the elastic forces in the balloon and the forces resulting from the image pixel intensity, are in equilibrium. The balloon forms a boundary around the object of interest. In the second phase of the segmentation process, the final shape of the object is obtained by fitting to the edge of the cell using an energy-minimizing spline (or 'snake') guided by external constraint forces and influenced by image forces that pull it toward edge features[5] (Online Methods).

We grew *Arabidopsis* on the surface of agar nutrient plates and maintained the plants upright between microscopy scans to avoid root bending. We constrained the orientation of the root tip using a coverslip, held in position by surface tension. Under these conditions, seedlings could be maintained healthy for 2–3 d. We followed easily recognizable cellular features during root growth by collecting three-dimensional image stacks over time. We could follow cells for up to 10 h across a series of images during time-lapse experiments by adjusting the focus plane of the stack during or after image collection (Online Methods and **Supplementary Movies 1** and **2**).

We tested the balloon-segmentation routine on a variety of images. Using this approach, we segmented cells in confocal microscopy images of plant tissues with irregular cell shapes, such as epidermal pavement cells from *Arabidopsis* leaves (**Supplementary Fig. 1a**). We also applied the method to images with reduced signal-to-noise ratios, such as internal cells of the root apical meristem (**Fig. 1g–j**) and wide-field microscopy images of *Coleocheate scutata* (**Supplementary Fig. 1b–e**). Comparison of balloon segmentation with other methods showed that the active contour segmentation routine was resistant to introduced noise and showed no major loss of performance after we artificially degraded 35% or 50% of pixels, whereas we saw failures in segmentation with watershed segmentation (**Supplementary Fig. 1f–m**). A priori knowledge of the position of nuclei improved the robustness of segmentation. Other techniques such as

[1]Department of Plant Sciences, University of Cambridge, Cambridge, UK. [2]The James Hutton Institute, Invergowrie, Dundee, Scotland, UK. [3]Institut de Recherche pour le Développement, Unité Mixte de Recherche, Diversité Adaptation Développement, Équipe Rhizogenèse, Montpellier, France. [4]Developmental Biology Unit, European Molecular Biology Laboratory, Heidelberg, Germany. [5]School of Biological Sciences, University of Sydney, Sydney, Australia. [6]These authors contributed equally to this work. Correspondence should be addressed to J.H. (jh295@cam.ac.uk).

RECEIVED 1 NOVEMBER 2011; ACCEPTED 2 FEBRUARY 2012; PUBLISHED ONLINE 1 APRIL 2012; DOI:10.1038/NMETH.1940

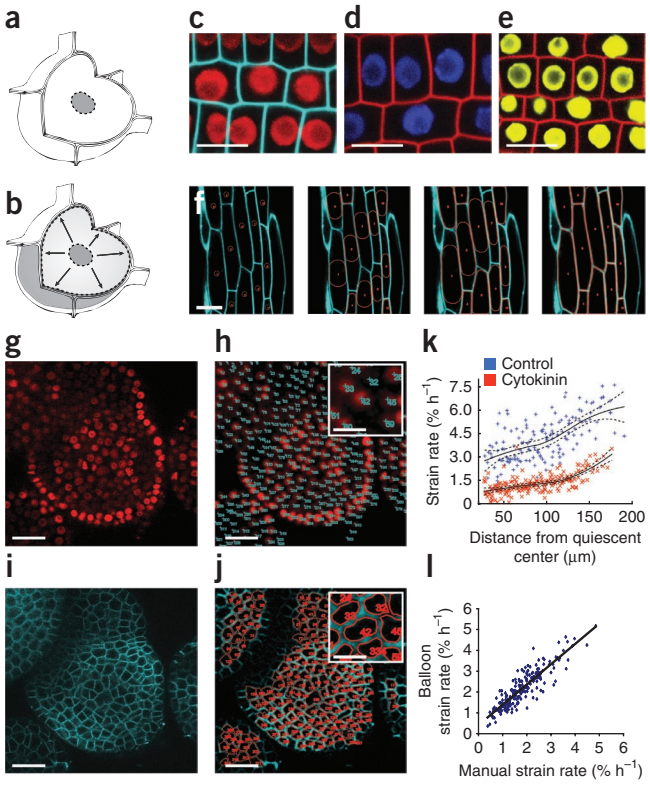

Figure 1 | Automated segmentation of cells in *Arabidopsis*. (**a**,**b**) Schematics of a transgenic plant cell used for *in planta* cytometry: a nuclear fluorescent protein is used for balloon 'seeding' and cell indexing (**a**), and a plasma membrane marker is used to obtain cell geometries (**b**). (**c**–**e**) Confocal microscopy images of *Arabidopsis* root meristem tissues containing *35S::H2B-mRFP1* and *35S::EGFP-LTI6b* (**c**), *35S::H2B-EYFP* and *35S::mCherry-LTI6b* (**d**) and *35S::H2B-ECFP* and *35S::mCherry-LTI6b* (**e**). Histone 2B fusions are localized to nuclei, LTI6b fusions are localized to the plasma membrane. (**f**) Step-by-step progress of balloon (red) inflation during the segmentation of epidermis cells of *Arabidopsis* hypocotyl. (**g**–**j**) Segmentation of cells in the shoot apical meristem of *Arabidopsis*. Confocal micrographs of a meristem (**g**) showing nuclear localization of H2B-mRFP1 protein; automated identification of labeled nuclei (**h**); plasma membrane–localized distribution of EGFP-LTI6b in the same plant (**i**); and automated segmentation of cells using individual mRFP1-labeled nuclei as seeds for balloon segmentation with EGFP labeled cell outlines (**j**). Scale bars, 40 μm (**g**–**j**) and 15 μm (**c**–**f** and insets in **h** and **j**). (**k**) Cell-expansion rates at indicated distance from the quiescent center in the root meristem in control and cytokinin-treated roots. Individual values for cortex cell strain rates were obtained from segmented image data. Solid lines indicate mean expansion rate and dashed lines, ± s.e.m. (n = 20). (**l**) Comparison of strain rate values obtained from the balloon segmentation technique and from manual measurements of cell size using ImageJ.

level sets[1], histogram shape–based[2] and entropy autothresholding[3] were also less accurate in noisy images. Threshold-based methods were the most efficient for cell segmentation in terms of calculation time but tended to oversegment images. The level-set method, a nonmarked active contour method, resulted in less deviation from manually segmented cells compared to thresholding and watershed methods, but remained susceptible to 'spilling' and was the least computationally efficient method of all.

As a proof of concept, we used *in planta* cytometry to study the effect of cytokinins on cell expansion in the root apical meristem and compared it to manual measurements of cellular properties. We treated *Arabidopsis* roots expressing *EGFP-LTI6b* (*LTI6b* is also known as *AT3G05890* and encodes a low temperature–induced protein) and *H2B-mRFP1* (*H2B* is also known as *AT5G22880* and encodes histone H2B), each under the control of a CaMV 35S promoter, with 0.1 μM *trans*-zeatin or a control solution. We tracked a cohort of cells for 10 h to analyze rates of cell expansion and measured cortex cell size manually or using balloon segmentation (**Supplementary Fig. 2a**–**h**). The analysis demonstrated that cytokinin application inhibited cell expansion in the root apical meristem and resulted in a threefold reduction in strain rate across the meristem. Automatic and manual measurements of cells produced similar estimates for cell size and strain rates (slope = 0.975, intercept = 0.0037, R^2 = 0.8) (**Fig. 1k**–**l** and **Supplementary Fig. 2i**). These results indicated that the automatic segmentation did not introduce substantial distortion and can provide reliable information for kinematic studies. The cellular architecture and arrangement of cells in the growing root was unaffected by the culture and time-lapse procedure. We measured strain rates of 3–5% h^{-1} in the apical few hundred micrometers of control root tips, which are similar to values of 4% h^{-1} obtained using bead tracking in growing roots[6].

The segmented nuclear regions used for balloon seeding can be used to obtain the average pixel intensity for the constitutive nuclear marker in the targeted cell. This can act as a reference value for normalization of additional colocalized fluorescent markers. We fused different regulated promoters to sequences encoding spectrally distinct fluorescent proteins targeted to the nucleus, and analyzed the resulting fluorescence signal with respect to a standard nuclear reporter expressed from the *35S* promoter (**Fig. 2**). Fluorescence signals in deeper tissues are attenuated by light scattering, absorbance and refraction. Ratiometric measurement allows normalization of fluorescence values and comparison of signals at different tissue depths (**Fig. 2a**–**d**). We visualized cellular responses to gravity-induced redistribution of auxin in *Arabidopsis* roots by imaging expression of the *DR5rev::3×Venus*-N7 (ref. 7) marker with respect to *35S::H2B-mRFP1* (**Fig. 2e**). The synthetic *DR5rev* promoter[7] has been widely used as an indicator of auxin response. We plotted the ratio of the expression of the markers encoded by the two constructs on tracings of cells in the root tip and epidermis (**Fig. 2f**,**g**). The shift of roots to the horizontal position triggered redistribution of auxin to the lower side of roots, as has been previously reported[8]. We examined *DR5rev* promoter activity in the cells of reoriented roots and found relative differences of up to 200-fold in DR5-regulated expression in epidermis cells of the elongation zone in the upper and lower portions of a root.

We also used *in planta* cytometry to classify root epidermal cells as hair cells and non–hair cells according to their size and response to the phytohormone auxin. It has been shown recently that a subset of epidermal cells, which later develop root hairs, accumulate less auxin than non–hair cells owing to the lack of AUX1 protein[9]. We created an auxin reporter line expressing the *IAA2* (*AT3G23030*) promoter fused to *H2B–mRFP1* sequence (*IAA2::H2B-mRFP1*) to study the response of root epidermis cells to auxin. We used *35S::H2B-EYFP* as a nuclear marker to normalize the *IAA2::H2B-mRFP1* auxin-responsive marker and to identify cells, whereas we used a third marker, *35S::EGFP-LTI6b*, to segment cells (**Fig. 2h**). We saw a sharp boundary between non–hair cells and hair cells based on auxin response.

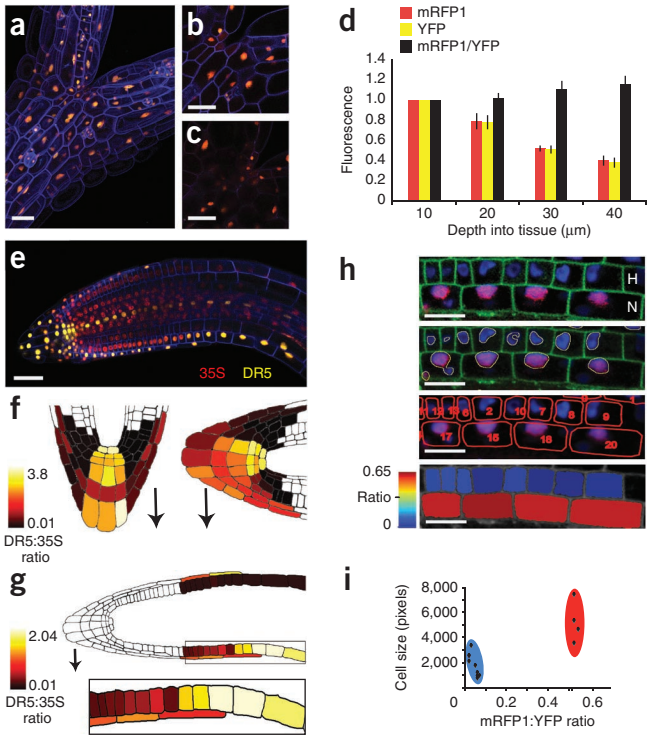

Figure 2 | Nuclear ratiometric measurements for in planta cytometry. (**a**) Confocal projection image of the hypocotl of a 4-day-old seedling expressing H2B–EYFP (green channel), histone H2B–mRFP1 (red channel) and EGFP-LTI6b (blue channel). (**b**,**c**) Confocal image sections at depths of 10 μm (**b**) and 40 μm (**c**). (**d**) Mean fluorescence intensity (arbitrary units) at indicated depths was normalized to values at 10 μm. Error bars, s.e.m. (n = 25 cells); similar data were obtained after analysis of 8 different seedlings. (**e**) Confocal image of the root of an *Arabidopsis* seedling containing auxin-responsive *DR5rev::3×Venus-N7* (labeled DR5) and a constitutive *35S::H2B-mRFP1* (labeled 35S), and imaged 6 h after shift to a horizontal orientation. (**f**,**g**) Relative levels of expression of the *DR5rev::3×Venus-N7* and *35S::H2B-mRFP1* markers was quantified and plotted on a tracing of the root cell outlines. Ratiometric measurement of auxin-responsive reporter gene expression in the root tip (**f**) before (left) and 6 h after (right) shift to a horizontal orientation and in the non–hair cells of the elongation zone 6 h after shift to a horizontal orientation (**g**). Arrows indicate the direction of gravitational force. (**h**) Confocal image of epidermal cells in the elongation zone of an *Arabidopsis* root expressing *IAA2::H2B-mRFP1*, *35S::H2B-EYFP* and *35S::EGFP-LTI6b* (top). Root hair (H) and non–root hair (N) cell files are indicated. Nuclear segmentation using the signal from *35S::H2B-EYFP* and cell outline after balloon segmentation are shown in the middle. The ratio of fluorescence signals from *IAA2::H2B-mRFP1* to *35S::H2B-EYFP*, visualized using a color map (bottom). (**i**) Ratiometric fluorescence values and size of cells from **h**. Cells with high mRFP1:EYFP ratios and larger cell sizes are indicated in red, cells with low mRFP1:EYFP ratios and smaller cell sizes in blue. Scale bars, 20 μm.

Non–hair cells responded more than hair cells, as measured by relative expression of the *IAA2::H2B-mRFP1* marker. Because non–hair cells are bigger than hair cells located at the same position in the longitudinal axis of the root, we could classify cells according to gene activity or cell size (**Fig. 2i**).

In planta cytometry has several benefits. First, the combined use of specific gene markers and active contour segmentation methods[5,10] allowed robust segmentation and fitting of cellular models to biological features such as nuclei and plasma membranes[11,12]. Second, active contour methods can be tailored for image analysis of features at a cellular scale, whereas watershed algorithm–based procedures require processing of an entire image. Third, the use of nuclear fluorescent markers also permitted implementation of nuclear ratiometric measurements (**Fig. 2**), enabling quantitative analysis of the relative contribution of multiple genes to cellular processes and correction for variability in marker fluorescence. The use of normalized units of measurement has aided the standardization and description of genes for design of predictable gene circuits in isolated cells and microbes[13]. Our work combines computational techniques and specific cellular markers to facilitate automatic identification and quantitative characterization of cells.

METHODS

Methods and any associated references are available in the online version of the paper at http://www.nature.com/naturemethods/.

Note: Supplementary information is available on the Nature Methods website.

ACKNOWLEDGMENTS

This research was supported by the Biotechnology and Biological Sciences Research Council, and Engineering and Physical Sciences Research Council research grants (BBS/B/16720 and BEP/17053 to J.H.), Institut de Recherche pour le Développement (L.L). F.F.'s PhD scholarship was supported by the Bill and Melinda Gates foundation (Gates Cambridge Trust). The Scottish Crop Research Institute receives grant-in-aid support from the Scottish Government Rural and Environment Research and Analysis Directorate (Workpackage 1.7). M.H. acknowledges the Australian Research Council for funding. We thank B. Scheres and H. Hofhuis (Utrecht University) for *DR5rev::3×Venus-N7* seeds and R.Y. Tsien (University of California, San Diego) for the *mRFP1* cassette.

AUTHOR CONTRIBUTIONS

F.F. generated the transgenic lines, analyzed the data and performed experiments. L.D. created the computational tools and plugin for ImageJ, and analyzed the data. J.H. provided instructions and supervision. M.H. performed confocal imaging of shoot apical meristem shown in **Figure 2** and **Supplementary Figure 1**. L.L. generated the pBI 35S::H2B-RFP binary vector and the *Arabidopsis 35S::H2B-RFP* transgenic line.

COMPETING FINANCIAL INTERESTS

The authors declare no competing financial interests.

Published online at http://www.nature.com/naturemethods/.
Reprints and permissions information is available online at http://www.nature.com/reprints/index.html.

1. Caselles, V., Kimmel, R. & Sapiro, G. *Int. J. Comput. Vis.* **22**, 61–79 (1997).
2. Otsu, N. *IEEE Trans. Syst. Man Cybern.* **9**, 62–66 (1979).
3. Kapur, J.N., Sahoo, P.K. & Wong, A.K.C. *Comput. Vis. Graph. Image Process* **29**, 273–285 (1985).
4. Rittscher, J. *Ann. Rev. Biomed. Eng.* **12**, 315–344 (2010).
5. Makowski, P. *et al. Comput. Med. Imaging Graph.* **26**, 9–17 (2002).
6. Beemster, G.T. & Baskin, T.I. *Plant Physiol.* **116**, 1515–1526 (1998).
7. Laskowski, M. *et al. PLoS Biol.* **6**, 307 (2008).
8. Ottenschläger, I. *et al. Proc. Natl. Acad. Sci. USA* **100**, 2987–2991 (2003).
9. Jones, A.R. *et al. Nat. Cell Biol.* **11**, 78–84 (2009).
10. Kass, M., Witkin, A. & Terzopoulos, D. *Int. J. Computer Vision* **1**, 321–331 (1988).
11. Mace, D.L. *et al. Bioinformatics* **22**, e323–e331 (2006).
12. Jönsson, H. *et al. Bioinformatics* **21** (suppl. 1), i232–i240 (2005).
13. Kelly, J.R. *et al. J. Biol. Eng.* **3**, 4 (2009).

ONLINE METHODS

Plant material. The *mRFP1* cassette was amplified by PCR using primers RFP5Eco 5′-CGGAATTCATGGCCTCCTCCGAG GAC-3′ and RFP3Sac 5′-CGGAGCTCTTAGGCGCCGGTGGA GTG-3′ introducing 5′ EcoRI and 3′ SacI restriction sites. This cassette was cloned in frame with the *Arabidopsis* histone H2B sequence in pBI35S::H2B-EYFP[14] giving rise to pBI35S::H2B-mRFP1. The pBI35S::H2B-RFP vector was digested by HindIII and EcoRI to remove the *35S::H2B* cassette as the *H2B* open reading frame contains two internal HindIII sites. This fragment was replaced by a synthetic multiple cloning site created by annealing primers A5 5′-AGCTCTCGAGCCCGGGGGAT CCG-3′ and A3 AATTCGGATCCCCCGGGCTCGAG-3′ *in vitro*. This removed the 5′ HindIII restriction site, introduced XhoI, SmaI and BamHI sites and maintained the 3′ EcoRI site. The H2B cassette was then amplified using primers H2B5 5′-CGGGGGACTCTAGAGGATCC-3′ and H2B3 5′-ACTGAATTCTCCAGCTCCAG-3′ to include 5′ BamHI and 3′ EcoRI sites and cloned back in frame with *mRFP1* in this new vector to generate the promoter-less pBIΔ::H2B-mRFP1 binary vector.

The *35S::mCherry-LTI6b* transgenic plants were created in *Arabidopsis* ecotypes C24 and Col-0. The *mCherry* gene was PCR-amplified from the Registry of Standard Biological Parts (http://partsregistry.org/) using the following oligonucleotides: forward 5′-AAGCCAACAATGGTGAGCAAGGGCGAGG-3′ and reverse 5′-AGCGGCCGCAGCCTTGTACAGCTCGTCCA TGCC-3′; and subsequently cloned into Zero Blunt PCR vector (Invitrogen). After sequencing, the mCherry gene was transferred to the pGEM-T-Easy vector (Promega), digested with BamHI and NotI enzymes and cloned into the BamHI and NotI sites flanking the *EGFP* sequence of the pBIB 35S-EGFP-LTI6b binary vector[15]. pBIB 35S::mCherry-LTI6b binary vector was used to transform *Arabidopsis* ecotypes C24 and Col-0 using the floral dip method. Positive seedlings were selected by red fluorescence using a Leica MZFLIII epifluorescence stereomicroscope.

The *35S::EGFP-LTI6b* and *35S::mCherry-LTI6b* lines were crossed to *35S::H2B-mRFP1*, *35S::H2B-ECFP* and *35S::H2B-EYFP* lines to obtain all the combinations of nuclear and plasma membrane markers. The *IAA2* auxin responsive promoter was PCR-amplified from genomic *Arabidopsis* DNA using the following oligonucleotides: forward 5′-CCCGGGCCTGCACTA TACACTTTCAAAAAGAG-3′ and reverse 5′-GGATCCGAGTTTT GGAGAAAAGGGGAG-3′; digested with BamHI and SmaI enzymes and subsequently cloned into BamHI and SmaI sites upstream of histone H2B gene in the pBIΔ::H2B-RFP binary vector.

Plant growth conditions and imaging. All seeds were surface-sterilized with 95% (v/v) ethanol for 5 min, followed by 10% (v/v) Parazone (commercial bleach) with 0.01% (v/v) Triton X-100 detergent for 5 min. After five washes in sterile distilled water, seeds were cold-treated for 2–5 d at 4 °C to synchronize germination, and then plated on Petri dishes containing 0.5× Murashige and Skoog (MS) basal salts (Melford), 0.5 g/l 2-(*N*-morpholino) ethanesulfonic acid (MES), 0.7% agar (Sigma), pH 5.8 and sealed with gas permeable tape. If required, zeatin (tZ; Sigma-Aldrich) was dissolved in sterile water, filter-sterilized and diluted from a 1,000× stock in autoclaved medium cooled to 50 °C. We prepared 1 mg/ml 1-NAA (α-napthaleneacetic acid) from a liquid solution (Sigma-Aldrich). We dissolved 10 μM 2,4-dichlorophenoxyacetic acid (2,4-D; Sigma-Aldrich) in sterile water, filter-sterilized and diluted from a 1000× stock. GA_3 (gibberellic acid; Duchefa) was dissolved in 50% (v/v) ethanol, filter-sterilized and a 1,000× stock dilution was used for each experiment.

All seeds were germinated and grown vertically in 0.5× MS under long day length light (16 h–8 h cycle) at 22 °C. For zeatin treatment, seeds were germinated in 0.5× MS and grown for 3.5 days before transfer to vertical Petri dishes containing 0.1 μM zeatin. After 16 h of treatment, 20 μl of MS liquid containing 0.1 μM zeatin or control solution was added to each root and gently covered with a coverslip. The experiments continued for 10 h after the addition of the coverslips and dishes were maintained vertical during intervals between microscopy scans to avoid root bending and thus maintaining the orientation of cells with respect to the focal plane. A simple procedure was followed to minimize fluctuations in the *z* plane during image collection over long time courses. (i) A feature was chosen that was easily recognizable in longitudinal section. In roots for example, a focal plane that provided a longitudinal optical section through the labeled nuclei of a median layer of the cortex could be reproducibly selected on a confocal microscope. (ii) A series of 10 optical sections were obtained from the region above and below this median section. It was sometimes necessary to manually adjust the focus of the microcope during a time course experiment, to follow cells growing at the curved tip of the root apex. (iii) The 3D stacks of images were used to manually identify the optimum optical section for each sample. Only roots that do not rotate or twist during time-lapse experiments were considered for analysis. The coverslips were held in position over tips of the roots by surface tension. Aliquots (20 μl) of 0.5× MS medium were regularly added to avoid dehydration and pressure on the root between the agar surface and coverslip. Under these conditions, seedlings could be maintained healthy for 2–3 d. This provided a simple and effective device for positioning and registration of growing *Arabidopsis* roots for long-term imaging experiments. The roots were growing over the surface of a vertically orientated nutrient agar plate, and showed no evident perturbation of root form. For NAA, and 2,4-D GA_3 treatments, seeds were germinated and grown in 0.5× MS and treated with 20-μl droplets containing the hormones or control solution. For GA_3 treatment, seeds were germinated and grown in 0.5× MS for 4 d before treated with 100 μM GA_3. After GA_3 application, roots were covered with a coverslip and imaged at the indicated different times.

Images were acquired as 8-bit TIFF files using a Leica TCS SP1 confocal laser scanning microscope with 40× NA 0.8 oil-immersion objective and pinhole equivalent to 1.5× the Airy disk diameter. EGFP and YFP were excited using the 488 nm and 514 nm lines of an argon ion laser, respectively, whereas mCherry and mRFP1 were excited using the 568-nm krypton laser. Fluorescence emission was detected at 505–530 nm for EGFP, 535-545 nm for EYFP and 606–635 nm for mCherry. Identical microscope settings were maintained during the experiments and clipping of pixel intensities was avoided. For time lapse experiments, images were acquired every 1 h. After acquisition of each image during a time-lapse experiment, the plates were sealed with tape to prevent desiccation and returned to the vertical position in the plant growth room. Multichannel images were merged in ImageJ (http://rsb.info.nih.gov/ij/), and unedited images were used for ratiometric analysis. Image levels were adjusted in Adobe Photoshop for presentation.

doi:10.1038/nmeth.1940

For cell-expansion analyses, two continuous side-to-side files of cortex cells were used and thus avoiding segmentation of cells that were not perfectly aligned with respect to the focus plane.

Balloon segmentation. The algorithm has been implemented as a Java ImageJ plugin, which can be freely downloaded (http://www.archiroot.org.uk/). A graphical interface has been provided to allow adjustment of the main parameters of the algorithm (**Supplementary Fig. 3**). Other properties, such as number of vertices, bending stiffness, initial balloon size, can be modified in configuration files. Before segmentation, images were processed to remove background noise. First, long-range modulations of the background intensity were removed using a boxcar averaging routine over a region of 20 square pixels (using the background removal function under ImageJ). Images were normalized and filtered with a Gaussian filter of radius 4 pixels to smooth images and reduce noise.

Robustness of segmentation was assessed by degrading cell wall signal using random black speckle of increasing intensity, representing successively 20%, 35% and 50% of the signal in the image.

We modeled the balloon geometry as a closed envelope. The balloon was decomposed into sections modeled as springs, which were bound together at their end points to form vertices. The springs are characterized by stiffness K, relaxation rate R, current length L and natural length L_0. Vertices have a mass m and are characterized by their position $\mathbf{M}$ and the velocity $\mathbf{V}$. The motion of vertices results from the action of forces in the two adjacent spring $\mathbf{F_{s1}}$ and $\mathbf{F_{s2}}$ forces, a constant inflation force $\mathbf{F_i}$ applied perpendicularly to the balloon surface, and the external image force $\mathbf{F_p}$:

$$\mathbf{F_{s1}} = K(L - L_0)\mathbf{n_{s1}}$$
$$\mathbf{F_i} = P_0\,\mathbf{n_N}$$
$$\mathbf{F_n} = -C_1 I\mathbf{n_N}/L \text{ or } C_2\,\Delta I\,\mathbf{n_N}/L$$

P_0 (pressure), C_1 and C_2 are constants. The segmentation can follow two steps. In the inflation stage $\mathbf{F_i}$ is not zero and external image forces are proportional to the image intensity (I) along the normal vector of the balloon ($\mathbf{n_N}$). In a second stage, optimal boundary detections can be obtain by suppressing inflation forces and using the image Laplacian (ΔI) as external image forces. Time is dimensionless and its unit will be denoted T for clarity. In order solve the physical equations for balloon deformation, time is discretised into steps, so that time t at the nth time step $t = ndt$.

Inelastic deformation is necessary to enable modelling of growth and formation of irregular shapes. This is implemented through a relaxation mechanism where the natural length of the spring varies as a function of the deformation state:

$$L_0^{t+dt} = R(L^t - L_0^t)dt$$

Inflation of the balloons causes the build up of forces perpendicular to each surface as well as the forces stored in the springs due to elastic deformation. These are computed and equilibrated at the end vertices (**Supplementary Fig. 4**). A forward finite difference scheme is then used to determine the displacement of the balloon vertices at time $t + dt$ using the conservation of momentum:

$$\mathbf{V}^{t+dt} = \mathbf{V}^t + \mathbf{F}^t dt/m$$

$$\mathbf{M}^{t+dt} = \mathbf{M}^t + \mathbf{V}^t dt$$

The model also takes into account bending stiffness K_b and viscous forces (υ) at the vertices. Balloons interact with each other to prevent overlap between neighboring balloons. The detection of contact is achieved by translating each vertex by small distance e (interface width) and checking for inclusion in neighboring balloons. If inclusion is detected for a given vertex, its movement is allowed only in parallel to the surface it is in contact with, following a perfectly smooth interaction model (**Supplementary Fig. 4b**).

In this model, image intensity is measured in units, for example, 0–255 in 8-bit images, and are assumed to be equivalent to a pressure (P_0 = 50 units). Forces are therefore measured in units pix. The dynamic parameters, such as viscosity or point mass, influence the convergence and stability of the algorithm but not the final shape of the balloon at equilibrium. We have chosen them empirically to maintain convergence and we kept them constant throughout our study: m = 1 units T^2; υ = 2 units T; dt = 0.02 T. The parameters we varied for segmenting the different types of cells are those acting on the resolution (number of vertices per pixel) and describing the resistance to balloon deformation: spring stiffness K (units) restrain the overall size of the segmented cell; the relaxation rate R (T^{-1}) allows cells of different shape and size to be segmented; bending stiffness influence the smoothness of the shape K_b (unit pix^2).

An ImageJ plugin has been developed to implement the balloon segmentation algorithm in two dimensions. It is distributed under the terms of the General Public License and is available at http://www.archiroot.org.uk/doku.php/navigation/architools/ and is available in the Fiji distribution of ImageJ.

A graphical interface has been developed which allows selection of regions of interest, location of cell centres, import and saving of results. Although all segmentation steps can be automated, manual intervention is possible through the different steps of the segmentation process. Settings for the segmentation algorithm are saved in properties files, and examples can be found on the plugin website.

Calculation of strain rate. The strain is a measure of deformation used in mechanics that quantify the relative displacement of material particles. The strain is a local measure that can be expressed, when deformations are small, as the ratio of the total deformation by the initial dimension of an object:

$$E = dL/L_0$$

This definition of strain is termed engineering or Cauchy strain[16]. When the small strain hypothesis is not true anymore, a non linear measure of the strain is used (obtained by integrating the engineering strain over the length of the object):

$$E = \ln(L + dL)/L_0$$

Strain rate is the change of strain with time and was calculated as

$$d\varepsilon/dt = \ln(L + dL)/(dtL_0)$$

where dt is the time interval between two images, and dL is the change with time of the balloon longitudinal dimension obtained by projecting the balloon vertices along the longitudinal axis.

Particle searching and tracking. Nuclei were processed using well known image-analysis techniques. Nuclei were automatically

identified by thresholding the image and applying a connected component algorithm. For analysis of particle movement, we used a particle-tracking algorithm developed previously[17] based on optimization (SpotTracker ImageJ plugin). We did not address the issue of cell division and tracking of lineage; there are, however, algorithms that allow this type of analysis[18].

14. Boisnard-Lorig, C. *et al. Plant Cell* **13**, 495–509 (2001).
15. Kurup, S. *et al. Plant J.* **42**, 444–453 (2005).
16. Boresi, A.P. & Chong, K.P. *Elasticity in Engineering Mechanics* (Wiley-IEEE, New York, 2000).
17. Sage, D., Neumann, F.R., Hediger, F., Gasser, S.M. & Unser, M. *IEEE Trans. Image Process.* **14**, 1372–1383 (2005).
18. Bao, Z. *et al. Proc. Natl. Acad. Sci. USA* **103**, 2707–2712 (2006).

doi:10.1038/nmeth.1940